# Phonon side bands in the absorption spectra of $Ni^{2+}$ and $Co^{2+}$ in $CdI_2$ and $PbI_2$

S. R. Kuindersma, P. R. Boudewijn, C. Haas, J. Bethlehem, and A. Meetsma
*Laboratory of Inorganic Chemistry, Materials Science Center of the University, Nijenborgh 16, 9747 AG Groningen, The Netherlands*
(Received 1 April 1981; revised manuscript received 28 September 1981)

The absorption and magnetic circular dichroism spectra of the $^3A_{2g} \rightarrow {}^1E_g$ electronic transition of $CdI_2$:$Ni^{2+}$ and $PbI_2$:$Ni^{2+}$ and of the $a^4T_{1g} \rightarrow b^2T_{1g}, {}^2A_{1g}$ transition of $CdI_2$:$Co^{2+}$ have been measured. The spectra show a complicated fine structure caused by the coupling with nonlocalized vibrational modes of the host lattice. The theory of this effect is presented. It is shown that the observed vibronic structure images the phonon density of states in the Brillouin zone, modified by matrix elements and selection rules. The contributions of the different phonon branches (acoustic, Raman, and infrared-active modes) are calculated. The spectra show a strong anisotropy, which is due to the presence of static dipoles at the anions; the magnitude of the anisotropy is calculated with use of the polarizable-ion model. The vibronic fine structure is used to deduce the maxima of the phonon density of states of $CdI_2$ and $PbI_2$, and to estimate the phonon dispersion curves.

## I. INTRODUCTION

$CdI_2$, $PbI_2$, and $CoI_2$ crystallize in the $Cd(OH)_2$ structure, $NiI_2$ in the $CdCl_2$ structure.[1] The unit cells of both structures can be described hexagonally with the $c$ axis as the uniaxial axis. Both structures consist of slabs $I$-$M$-$I$; the slabs are interacting only weakly by van der Waals forces. The metal ion is octahedrally surrounded by six iodine ions. In the diluted systems part of the Cd or Pb ions is replaced by $Co^{2+}$ or $Ni^{2+}$.

Optical absorption spectra of the first-row transition-metal diiodides in the visible and near-infrared wavelength region exhibit localized $d$-$d$ transitions. The pure transition-metal diiodides, especially $NiI_2$ and $CoI_2$ also show a strong absorption, due to charge-transfer transitions, which overlap many of the much weaker forbidden $d$-$d$ transitions.

The $d$-$d$ transitions of transition-metal ions substituted on sites with inversion symmetry are parity forbidden for electric-dipole transitions. They become allowed in optical absorption by means of a coupling with vibrations of odd parity. In these cases the zero-phonon transition is observed as a weak magnetic-dipole transition. The electric-dipole transitions occur as vibronic side bands.

In the literature there are numerous examples of complicated vibronic fine structures, simple phonon progressions, and combinations of both phenomena. The type of vibronic side band that is observed, depends strongly on the magnitude of the lattice distortion and of the vibronic coupling. Bron and Wagner[2] distinguished four combinations of the magnitude of the lattice distortions due to the ion substitution and the electron-phonon coupling. A small lattice distortion and a weak coupling lead to one-phonon processes, as observed for instance for intraconfigurational transitions $4f^n \rightarrow 4f^n$ of $Pr^{3+}$ in $LaCl_3$.[3] The observed maxima in this spectrum are ascribed to singular points in the Brillouin zone of $LaCl_3$, and the spectrum reflects the phonon density of states of $LaCl_3$, modified by vibronic selection rules.

For crystals with defects (substituted ions) the influence of the defect atom on the vibrational modes should be taken into account. Not only mass defects should be considered but also changes in the force constants.[4]

The crystal-field transitions of the systems CaO:$Ni^{2+}$ have been investigated in great detail.[5,6] Because $Ca^{2+}$ has been replaced by the heavier $Ni^{2+}$ ion and the force constants with nearest-neighbor ions are likely to be reduced, a resonant mode is expected. Electric-dipole transitions from the ground state $^3A_{2g}(t_{2g}^6e_g^2)$ to the excited states $^1T_{2g}(t_{2g}^5e_g^3)$, $^3T_{1g}(t_{2g}^5e_g^3)$ show a number of peaks at the low-frequency sides of broad bands. These peaks are ascribed to a vibronic coupling of the electronic states with a resonant mode of $t_{1u}$ symmetry.

Sangster and McCombie[7] have considered the emission spectrum of the $^2E_g(t_{2g}^3) \rightarrow {}^4A_{2g}(t_{2g}^3)$ transition of $V^{2+}$ in MgO. A comparison of the phonon side bands of electronic transition in MgO:$Ni^{2+}$ and MgO:$V^{2+}$ shows that the bands are very sensitive to modifications of the modes in the immediate vicinity of the defect ion. Three localized $t_{1u}$ modes were taken into account; one $t_{1u}$ modulates the transition metal-ligand distance, the second changes the ligand-

metal-ligand angle and the third is a translational mode. The response of the lattice to the change of the mass and the force constants has been evaluated with a Green's function method. Only displacements of the impurity ion and its nearest neighbors were coupled to the electronic transition. The largest contribution appeared to arise from the localized $t_{1u}$ which modulates the metal-ligand distance.

In this article we discuss the absorption and magnetic circular dichroism (MCD) spectra of the isoconfigurational transition $^3A_{2g}(t_{2g}^6e_g^2) \rightarrow {}^1E_g(t_{2g}^6e_g^2)$ in $CdI_2$:$Ni^{2+}$ (Ref. 8) and $PbI_2$:$Ni^{2+}$ and related transitions in $CdI_2$:$Co^{2+}$.[9,10] The spectra show zero-phonon magnetic-dipole transitions and fine structures due to vibronic side bands. The fine structure can be related to the phonon density of states of the host lattice. The general theory of the coupling of parity-forbidden electronic transitions located at the defect ion, with the vibrational modes of the host lattice is given. The theory is applied to layered diiodides; the anisotropy of the coupling is attributed to the vibrational anisotropy of the layered compounds. The contributions of the various phonon branches in the Brillouin zone to the fine structure in the spectra are calculated. Finally, the maxima in the fine structures are assigned to the maxima in the phonon density of states, which corresponds to flat regions of the dispersion curves near symmetrical points in the Brillouin zone. Tentative dispersion curves of $CdI_2$ are estimated from the assignments of the spectra.

## II. EXPERIMENTAL PART

$CdI_2$, $PbI_2$, $NiI_2$, and $CoI_2$ were prepared from the elements in evacuated quartz ampoules at temperatures of 350, 470, 700, and 500 °C, respectively. Also commercial $CdI_2$ was used after sublimation at about 450 °C. The solid solutions were synthesized with the Bridgman technique. A powder of $CdI_2$ or $PbI_2$ was mixed with a small amount of $NiI_2$ or $CoI_2$, and put in a small quartz tube. The evacuated tubes were kept for several days at a temperature of 450 °C in the case of $CdI_2$ or at 500 °C in the case of $PbI_2$, and then carefully lowered through the temperature gradient. From the ingots it is easy to cut single-crystal plates perpendicular to the $c$ axis; these plates are used for recording the axial spectra. In order to obtain crystal plates with the $c$ axis parallel to the crystal plane, the samples were embedded in a two component thermosetting resin (Buehler). The crystals were carefully sawn with a diamond saw. Some of the crystals were polished with powders, other crystals were cleaned with an ethanol-wet wash leather. The optical quality of these crystals is less than that of the naturally cut crystals, used for the axial spectra.

The $3d$-metal ion concentration was determined by chemical analysis. In the $CdI_2$:$Co^{2+}$ samples the $Co^{2+}$ concentration varied from 0.5 to 0.88 mol%. The $CdI_2$:$Ni^{2+}$ crystal contained 0.1 mol% of $NiI_2$. The chemical analysis of $PbI_2$:$Ni^{2+}$ revealed a concentration as large as 2.0 mol% $NiI_2$. A microscopic study, however, showed the presence of some dark rings, probably due to an enhanced local concentration of Ni.

The transmission and MCD spectra were recorded with a Perkin-Elmer E-1 monochromator. The sample was mounted in an Oxford Instruments SM 4 cryostat, providing magnetic fields up to 5 T. The temperature was varied from 1.5 to 300 K. The resolution was about 2 $cm^{-1}$.

In Fig. 1 the absorption ($\alpha$, $\pi$ polarized) and MCD spectra at 4.2 K of the $^3A_{2g} \rightarrow {}^1E_g$ transition of

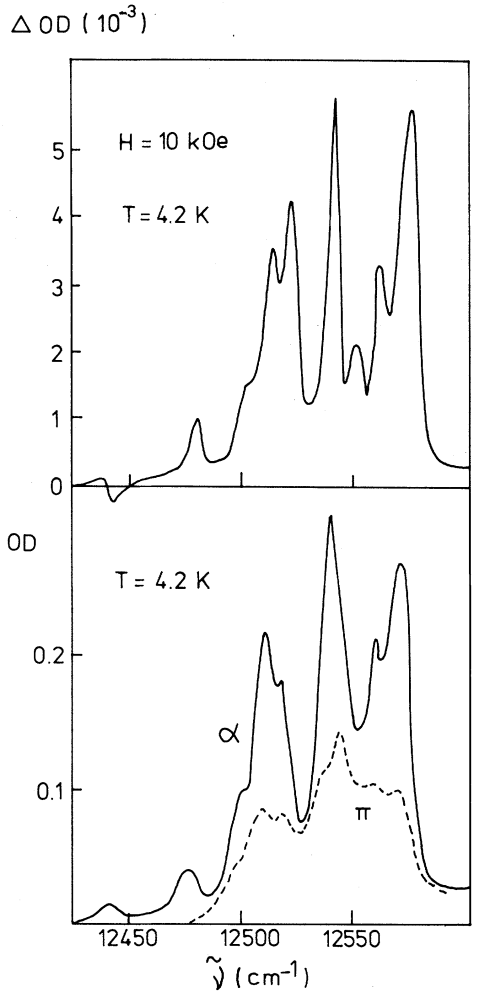


FIG. 1. Absorption (lower part) and MCD spectra (upper part) of the $^3A_{2g} \rightarrow {}^1E_g$ transition in $CdI_2$:$Ni^{2+}$ at 4.2 K. The figure gives the optical density (OD) and ΔOD as a function of photon energy. The magnetic field of the MCD is 10 kG. The solid curve is the $\alpha$- and the broken curve is the $\pi$-polarized absorption.

$CdI_2$:$Ni^{2+}$ are shown. The absorption spectra were recorded for the configurations $\alpha(\vec{E}\perp c, \vec{H}\perp c)$, $\pi(\vec{E}\parallel c, \vec{H}\perp c)$, and $\sigma(\vec{E}\perp c, \vec{H}\parallel c)$. The MCD spectrum was recorded with the light propagating along the $c$ axis and the magnetic field parallel to the $c$ axis. The absorption spectrum changes only slightly between 4.2 and 30 K; above 30 K a broadening is observed. The observed sharp features with splittings of a few wave numbers do not correspond to the known frequencies at $\vec{k}=0$ of $CdI_2$. Striking is the different shape of the bands at 12 441 and 12 478 $cm^{-1}$. Whereas the band at 12 441 $cm^{-1}$ is symmetric, the band at 12 478 $cm^{-1}$ has a long tail to lower energies. Another remarkable feature is the sharp cutoff of the spectra at about 12 600 $cm^{-1}$.

There is a reduction of the intensities in the $\pi$-polarized spectrum as compared with those of the $\alpha$ polarization. The positions of the peaks in both spectra coincide. An exception is the behavior of the band at 12 544 $cm^{-1}$, the intensity of which does not reduce from $\alpha$ to $\pi$.

The MCD spectrum consists of temperature-dependent $C$ terms.[11] The band at 12 441 $cm^{-1}$ has an opposite sign to that of the rest of the spectrum, and is assigned to the zero-phonon magnetic-dipole transition. A comparison of the linewidth of the bands at 12 540 and 12 544 $cm^{-1}$ in absorption and MCD indicates that the MCD consists of two contributions of opposite sign.

In Fig. 2 the absorption ($\alpha$ polarized) and MCD

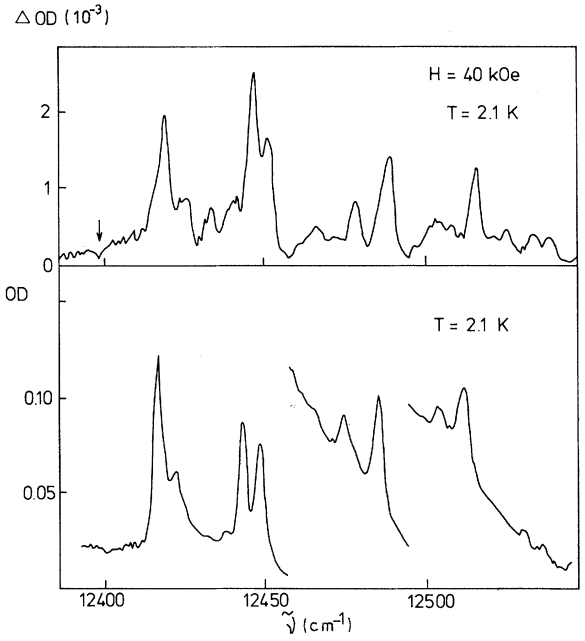


FIG. 2. Absorption (lower part) and MCD spectra (upper part) of the ${}^3A_{2g}\rightarrow{}^1E_g$ transition in $PbI_2$:$Ni^{2+}$ at 2.1 K. The figure gives the OD and ΔOD vs photon energy. The absorption is $\alpha$ polarized. The magnetic field of the MCD is 40 kG.

spectra at 2.1 K of $PbI_2$:$Ni^{2+}$ are shown. The frequency region is the same as for $CdI_2$:$Ni^{2+}$, and the fine structure is assigned to the ${}^3A_{2g}\rightarrow{}^1E_g$ transition. Although a chemical analysis of $PbI_2$:$Ni^{2+}$ crystals revealed a $Ni^{2+}$ concentration of 2 mol% we believe that the local concentration is much lower. The absorption and MCD signals are much weaker than those of $CdI_2$:$Ni^{2+}$ (0.1 mol%).

The spectra of the $PbI_2$:$Ni^{2+}$ again show sharp vibronic features. The width of the spectrum is about 120 $cm^{-1}$. Apart from the sharp peaks in the absorption spectrum, there is a broad background. This background is not observed in the MCD spectrum; the background was absent in crystals with a much lower $Ni^{2+}$ concentration.

$\sigma$- and $\pi$-polarized absorption spectra of $PbI_2$:$Ni^{2+}$ showed the same absorption peaks as the $\alpha$-polarized spectrum. However, the signal-noise ratio and resolution was bad. The maxima in the MCD spectrum correspond to the maxima in the $\alpha$-polarized absorption spectrum. The band at 12 394 $cm^{-1}$ (Fig. 2) has a MCD sign opposite to that of the rest of the spectrum, and is assigned to the zero-phonon transition.

Figures 3 and 4 show the $\sigma$- and $\pi$-polarized spectra of spin-forbidden transitions in $CdI_2$:$Co^{2+}$ (0.88 mol%). A detailed assignment of the $CdI_2$:$Co^{2+}$ spectra is reported in another publication.[10] Figure 3 shows the $a^4T_{1g}(t_{2g}^5e_g^2)\rightarrow b^2T_{1g}(t_{2g}^5e_g^2)$ transition of the $Co^{2+}$ ion ($d^7$). The excited state is split by spin-orbit coupling into two components $U_g'$ and $E_g'$; the zero-phonon transitions are observed at 15 280 $cm^{-1}$ and 15 376 $cm^{-1}$, respectively. The irregular pattern is originating from the phonon density of states of $CdI_2$. The spectrum of the $E_g'$ is a repetition of the spectrum of the $U_g'$, although it is much weaker. Figure 3 shows the strong reduction in intensity from $\sigma$ to $\pi$ polarization.

Figure 4 shows the vibronic fine structure of the

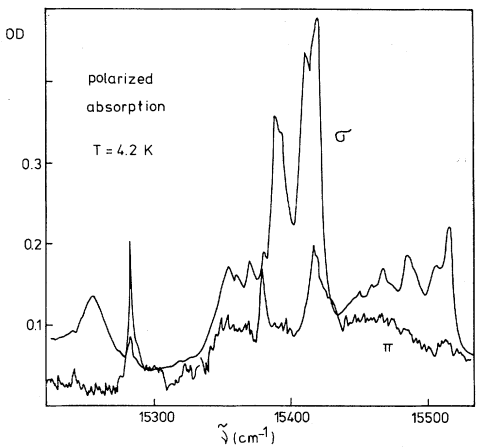


FIG. 3. Polarized absorption spectra of the $a^4T_{1g}\rightarrow b^2T_{1g}$ transition in $CdI_2$:$Co^{2+}$ at 4.2 K.

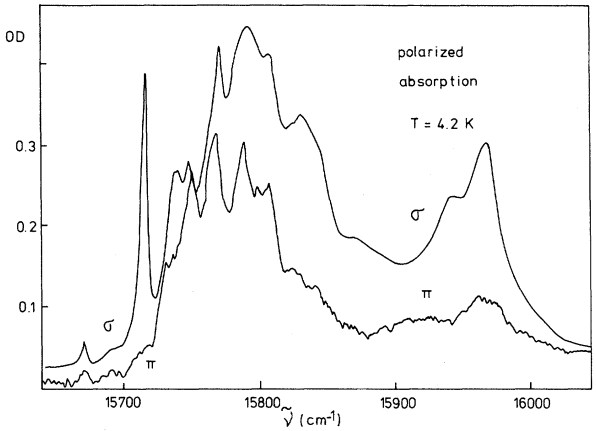


FIG. 4. Polarized absorption spectra of the $a^4T_{1g} \rightarrow {}^2A_{1g}$ transition in $CdI_2:Co^{2+}$ at 4.2 K.

$a^4T_{1g}(t_{2g}^5e_g^2) \rightarrow {}^2A_{1g}(t_{2g}^4e_g^3)$ transition. The band at 15 669 $cm^{-1}$ is assigned to the magnetic-dipole transition. The maxima in the vibronic side band of the $\sigma$ spectrum are broadened with respect to those in the spectrum of Fig. 3. The sharp cutoff at the high-frequency side (Figs. 1 and 3), characteristic for one-phonon processes, is not observed for the ${}^2A_{1g}$ transition. This is presumably due to two-phonon processes. An additional peak is observed at 15 716 $cm^{-1}$. Whereas the fine structure shows a reduction from $\sigma$ to $\pi$ polarization, the peak at 15 716 $cm^{-1}$ is completely $\sigma$ polarized.

Lists of observed positions of the maxima in the doped $CdI_2$ and $PbI_2$ systems are given in Sec. IV, together with the assignments to special points in the Brillouin zone.

## III. THEORETICAL PART

### A. General theory of vibronic coupling

In this section we discuss the complex problem of the coupling of the many-electron states of a transition metal with the vibrations of the crystal in which the ion is incorporated as an impurity.

The total Hamiltonian for this problem contains terms representing the electron-electron interaction, the spin-orbit coupling and the vibronic interaction between the electrons and the vibrations of the crystal. We consider transitions involving electrons which have predominantly $3d$ character. In that case the electron-electron interaction is strong and should be treated exactly. The spin-orbit interaction for $3d$ electrons is small and can be treated as a perturbation.

In the spirit of the Born-Oppenheimer approximation the total wave function can be written as a product of a many-electron wave function $\psi$ and a vibrational wave function $\chi$ (Ref. 12):

$$\Psi = \psi(\vec{r}_i, \vec{R}_k)\chi(\vec{R}_k) \ , \tag{1}$$

where $\vec{r}_i$ and $\vec{R}_k$ are the coordinates of the electrons and the nuclei, respectively.

We consider only vibrations of small amplitude around the equilibrium nuclear configuration $\vec{R}_k^0$, which we assume to be the same for all electronic states to be considered. The latter is a reasonable assumption for the discussion of transitions between isoconfigurational electronic states. In this approximation the vibrations are independent of the electronic state, and are in the harmonic approximation characterized by normal coordinates for independent harmonic vibrations. For an unperturbed crystal the normal coordinates $Q_{ki}$ are delocalized, and are characterized by a wave vector $\vec{k}$ ($i$ denotes the vibrational branch number). For a crystal containing an impurity ion one distinguishes delocalized modes $Q_{ki}$, derived from the normal modes of the unperturbed crystal, and local (gap) modes $Q_l$[4]. The normal coordinates $Q_{ki}$ are similar to those of the unperturbed crystal, except for the immediate vicinity of the impurity atom.

We consider an optical electric-dipole transition between two electronic states $a$ and $b$; the transition moment for light polarized with the electric vector in the $\beta$ direction, is given by

$$m_{ab}^{\beta} = \left\langle \psi_a \chi_a \middle| \sum_i m_\beta(\vec{r}_i) \middle| \psi_b \chi_b \right\rangle \ , \tag{2}$$

where $m_\beta(\vec{r}_i)$ are the components of the electronic dipole operator $\vec{m} = e\vec{r}_i$. The electronic transition moments for a fixed configuration of the nuclei $\vec{R}_k$ is

$$P_{ab}^{\beta}(\vec{R}_k) = \left\langle \psi_a(\vec{r}_i, \vec{R}_k) \middle| \sum_i m_\beta(\vec{r}_i) \middle| \psi_b(\vec{r}_i, \vec{R}_k) \right\rangle \ . \tag{3}$$

For a $d$-$d$ transition of a transition-metal ion at a site with inversion symmetry, $P_{ab}^{\beta}$ vanishes for the equilibrium nuclear configuration. Therefore, in order to obtain a nonvanishing transition probability, it is necessary to consider first-order terms linear in the nuclear displacements.

For a transition-metal atom in an octahedral coordination it is expected that the vibronic coupling will be predominantly with $t_{1u}$ local displacements of the octahedron of ligand atoms, which modulate the metal-ligand distance.[7,13,14]

If only the interaction with this type of displacements is considered, we obtain in first approximation for the vibronic interaction

$$H_v = \sum_\rho \Delta U_\rho^{t_{1u}}(\vec{r}_1 \cdots \vec{r}_i) q_{-\rho}^{t_{1u}} \ , \tag{4}$$

where $q_{-\rho}$ is the amplitude of the $t_{1u}$-type displacements with components $\rho=0, \pm 1$.

With these assumptions it is possible to evaluate the electronic-transition matrix elements $P_{ab}^{\beta}$ with perturbation theory, treating the spin-orbit interaction $H_{so}$ and the vibronic interaction $H_v$ as small perturbations. These matrix elements are quite complicated for the many-electron wave functions involved, and can be evaluated with use of the irreducible tensor method[15] (Sec. III B).

The electronic-transition matrix element depends linearly on the local amplitudes $q_{-\rho}$

$$P_{ab}^{\beta}=\sum_{\rho} B_{ab}^{\beta\rho} q_{-\rho} \ . \tag{5}$$

The local distortions can be decomposed into normal vibrations of the crystal:

$$q_{\rho}=\sum_{k}\sum_{i} S_{ki}^{\rho} Q_{ki}+\sum_{l} S_{l}^{\rho} Q_{l} \ . \tag{6}$$

The absorption coefficient $\alpha(\omega)$ for a transition $a \rightarrow b$ at low temperature, when all phonon modes $(\vec{k},i)$ are in the vibrational ground state $n_{ki}=0$, $n_l=0$ is given by

$$\alpha_{\beta}(\omega)=c\sum_{a\rightarrow b}\left(\sum_{k}\sum_{i}|\langle n_{ki}=0|P_{ab}^{\beta}|n_{ki}=1\rangle|^2\delta(\omega=\omega_0+\omega_{ki})+\sum_{l}|\langle n_l=0|P_{ab}^{\beta}|n_l=1\rangle|^2\delta(\omega=\omega_0+\omega_l)\right) \ , \tag{7}$$

where $c$ is a constant, $\beta$ gives the polarization direction of the light, and the summation is over all components of ground-state $a$ and excited electronic state $b$. The frequency $\omega_0$ corresponds to the zero-phonon energy separation of initial and final state. Using $\langle n=0|Q|n=1\rangle=(\hbar/2\omega)^{1/2}$ for a harmonic oscillator of frequency $\omega$, one obtains

$$\alpha_{\beta}(\omega)=c\sum_{a\rightarrow b}\sum_{\rho\rho'}(B_{ab}^{\beta\rho})^{*}(B_{ab}^{\beta\rho'})\left(\sum_{ki}\frac{\hbar}{2\omega_{ki}}(S_{ki}^{\rho})^{*}(S_{ki}^{\rho'})\delta(\omega=\omega_0+\omega_{ki})+\sum_{l}\frac{\hbar}{2\omega_l}(S_l^{\rho})^{*}(S_l^{\rho'})\delta(\omega=\omega_0+\omega_l)\right) \ . \tag{8}$$

From this expression the shape of the absorption spectrum can be calculated, if the coefficients $S_{ki}^{\rho}$ and $S_l^{\rho}$ are known.

### B. Theory of the $^3A_{2g}\rightarrow{}^1E_g$ electronic transition of $Ni^{2+}$ in an octahedral coordination

In this section we consider the electronic transition $^3A_{2g}\rightarrow{}^1E_g$ of a $Ni^{2+}$ ion in an octahedral coordination of ligand ions. Both the ground-state $^3A_{2g}$ and the excited-state $^1E_g$ are derived from the same strong-field configuration $t_{2g}^6e_g^2$. Thus the $^3A_{2g}\rightarrow{}^1E_g$ transition is isoconfigurational. One expects only a weak electron-phonon coupling, and no appreciable Franck-Condon effect.

The $^3A_{2g}\rightarrow{}^1E_g$ transition is allowed as a magnetic-dipole transition through spin-orbit coupling of the excited state with the $^3T_{2g}$ state. For low magnetic field ($g\mu_BH \ll kT$) the magnetic circular dichroism (MCD) is proportional to[11]

$$\sum_{a\rightarrow b}\langle a|\mu_z|a\rangle(|\langle a|\mu_+|b\rangle|^2-|\langle a|\mu_-|b\rangle|^2) \ , \tag{9}$$

where $\mu_z$ and $\mu_{\pm}$ are the magnetic moment operators. The summation is over all components of ground and excited state. For the $^3A_{2g}\rightarrow{}^1E_g$ magnetic dipole transition a negative MCD signal is calculated.

In the case of spin- and parity-forbidden electric-dipole transitions the spin-orbit coupling and the vibronic coupling together provide a number of mechanisms through which the transition may become allowed. With use of the pertubation theory, the relative importance of different processes can be estimated by comparing the energy denominators, which appear in the expressions for the transition probability. As a result of the relative closeness of the $^1E_g$ and the $^3T_{1g}$ and $^3T_{2g}$ states we have limited our calculations to the two processes depicted in Fig. 5. If one assumes that the dominant part comes from $t_{1u}$ vibrations, as is observed in other $Ni^{2+}$ systems,[13,14] the intermediate states $^3\Gamma_u$ will be $^3T_{2u}$. The transition moment for coupling with $^3T_{2g}$ is given by

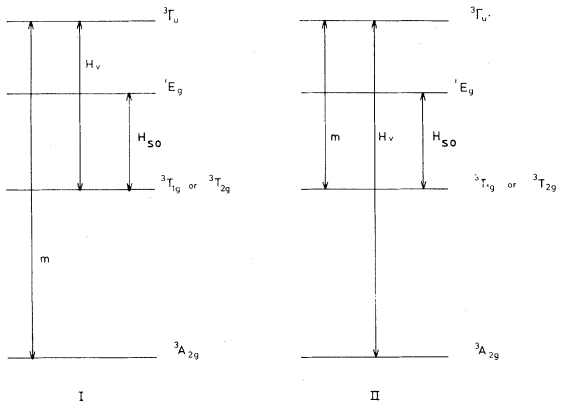


FIG. 5. Vibronic and spin-orbit coupling mechanisms, which make the $^3A_{2g}\rightarrow{}^1E_g$ transition in $CdI_2$:$Ni^{2+}$ electric dipole allowed.

$$\langle T_{2g}(^3A_{2g})\gamma\nu(a_{1g})\iota|m_\beta|E_g(^1E_g)\gamma'\nu(t_{1u})\tau\rangle$$

$$=\sum_\kappa\sum_{M_s}\sum_\rho\left[\langle T_{2g}(^3A_{2g})\gamma|m_\beta|^3T_{2u}M_s\kappa\rangle\langle{}^3T_{2u}M_s\kappa|\Delta U_\rho^{t_{1u}}|E_g(^3T_{2g})\gamma'\rangle\frac{1}{E(^3T_{2g})-E(^3T_{2u})}\right.$$

$$\left.+\langle T_{2g}(^3A_{2g})\gamma|\Delta U_\rho^{t_{1u}}|^3T_{2u}M_s\kappa\rangle\langle{}^3T_{2u}M_s\kappa|m_\beta|E_g(^3T_{2g})\gamma'\rangle\frac{1}{E(^3A_{2g})-E(^3T_{2u})}\right]$$

$$\times\frac{\langle E_g(^3T_{2g})\gamma'|H_{so}|E_g(^1E_g)\gamma'\rangle\langle a_{1g}\iota|q_{-\rho}^{t_{1u}}|t_{1u}\tau\rangle}{E(^1E_g)-E(^3T_{2g})}\ . \tag{10}$$

The states are labeled by their $O_h^*$ double-group representation, within brackets the $O_h$ representation. Vibrational states are indicated by $\nu(a_{1g})$ and $\nu(t_{1u})$ for ground and excited state, respectively (low-temperature approximation with only the lowest vibrational level of the ground-state populated). By use of $V$ coefficients the coupled functions $T_{2g}(^3A_{2g})\gamma$ and $E_g(^3T_{2g})\gamma'$ can be expressed in the uncoupled functions.[15] Integration over the spin coordinates and by using the Wigner-Eckart theorem make it possible to express the result in terms of $V$ coefficients and reduced matrix elements. The $V$ coefficients for the complex trigonal component system are given in Ref. 15. The result is

$$\langle T_{2g}(^3A_{2g})\gamma\nu(a_{1g})\iota|m_\beta|E_g(^1E_g)\gamma'\nu(t_{1u})\tau\rangle=\sum_{M_s}\sum_j-\frac{1}{\sqrt{6}}V\begin{pmatrix}A_{2g}&T_{1g}&T_{2g}\\ \iota&M_s&-\gamma\end{pmatrix}V\begin{pmatrix}T_{2g}&T_{1g}&E_g\\ j&M_s&-\gamma'\end{pmatrix}\epsilon_{\beta j\tau}M_2\ , \tag{11}$$

where we have used the fact that the matrix element of the spin-orbit coupling operator is $\frac{1}{2}\zeta'\sqrt{6}$ and

$$M_2=\zeta'(\langle{}^3A_{2g}||m||{}^3T_{2u}\rangle\langle{}^3T_{2u}||\Delta U^{t_{1u}}||{}^3T_{2g}\rangle/\Delta E_1$$
$$+\langle{}^3A_{2g}||\Delta U^{t_{1u}}||{}^3T_{2u}\rangle\langle{}^3T_{2u}||m||{}^3T_{2g}\rangle/\Delta E_2)\langle a_{1g}||q^{t_{1u}}||t_{1u}\rangle/\Delta E_3\ , \tag{12}$$

with

$$\Delta E_1=E(^3T_{2g})-E(^3T_{2u}),\quad \Delta E_2=E(^3A_{2g})-E(^3T_{2u}),\quad \Delta E_3=E(^1E_g)-E(^3T_{2g})\ . \tag{13}$$

The expressions obtained for coupling with the $^3T_{1g}$ are

$$\langle T_{2g}(^3A_{2g})\gamma\nu(a_{1g})\iota|m_\beta|E_g(^1E_g)\gamma'\nu(t_{1u})\tau\rangle=\sum_{M_s}\sum_j-V\begin{pmatrix}A_{2g}&T_{1g}&T_{2g}\\ \iota&M_s&-\gamma\end{pmatrix}V\begin{pmatrix}T_{1g}&T_{1g}&E_g\\ j&M_s&-\gamma'\end{pmatrix}V\begin{pmatrix}T_{1g}&T_{1u}&T_{2u}\\ j&\beta&\tau\end{pmatrix}M_1 \tag{14}$$

with

$$M_1=\zeta'\{\langle{}^3A_{2g}||m||{}^3T_{2u}\rangle\langle{}^3T_{2u}||\Delta U^{t_{1u}}||{}^3T_{1g}\rangle/\Delta E_1'$$
$$+\langle{}^3A_{2g}||\Delta U^{t_{1u}}||{}^3T_{2u}\rangle\langle{}^3T_{2u}||m||{}^3T_{1g}\rangle/\Delta E_2\}\langle a_{1g}||q^{t_{1u}}||t_{1u}\rangle/\Delta E_3' \tag{15}$$

and

$$\Delta E_1'=E(^3T_{1g})-E(^3T_{2u}),\quad \Delta E_3'=E(^1E_g)-E(^3T_{1g})\ . \tag{16}$$

The calculated transition intensities for the components of the $^3A_{2g}\rightarrow{}^1E_g(t_{1u})$ transition for different polarizations are given in Table I. Knowing that the lowest Zeeman level is the $^3A_{2g}-1$ component, the sign of the MCD is easily calculated; it is found that coupling with $^3T_{1g}$ results in a positive MCD signal, coupling with $^3T_{2g}$ in a negative MCD signal. The observed positive MCD signal for vibronic side bands indicates that spin-orbit coupling with $^3T_{1g}$ dominates, which is not surprising in view of the small energy difference between $^1E_g$ and the $^3T_{1g}$ state.[16]

TABLE I. Transition intensities for the $^3A_{2g} \rightarrow {}^1E_g(t_{1u})$ transition. The numbers in brackets give the component of the $t_{1u}$ vibration involved in the transition.

| | Coupling with $^3T_{1g}$ (in units of $A = M_1^2/324$) | | Coupling with $^3T_{2g}$ (in units of $B = M_2^2/108$) | |
|---|---|---|---|---|
| | $^1E_g+1$ | $^1E_g-1$ | $^1E_g+1$ | $^1E_g-1$ |
| $m_+$ | | | | |
| −1 | $A(0)$ | $A(+1)$ | $B(0)$ | $B(-1)$ |
| $^3A_{2g}$ 0 | $4A(-1)$ | $A(0)$ | 0 | $B(0)$ |
| +1 | $A(+1)$ | $4A(-1)$ | $B(-1)$ | 0 |
| $m_-$ | | | | |
| −1 | $4A(+1)$ | $A(-1)$ | 0 | $B(+1)$ |
| $^3A_{2g}$ 0 | $A(0)$ | $4A(+1)$ | $B(0)$ | 0 |
| +1 | $A(-1)$ | $A(0)$ | $B(+1)$ | $B(0)$ |
| $m_0$ | | | | |
| −1 | $A(-1)$ | $4A(0)$ | $B(+1)$ | 0 |
| $^3A_{2g}$ 0 | $A(+1)$ | $A(-1)$ | $B(-1)$ | $B(+1)$ |
| +1 | $4A(0)$ | $A(+1)$ | 0 | $B(-1)$ |

### C. Vibronic coupling in $Cd(OH)_2$-type layered compounds

In this part we discuss the lattice vibrations of crystals with the $Cd(OH)_2$-type structure, and the vibronic coupling of these vibrations with electronic transitions at an impurity ion.

The unit cell of the $Cd(OH)_2$-type structure contains two anions and one metal ion. A factor-group analysis yields nine normal modes $Q_i$ at $k=0$ (Fig. 6). Three modes are acoustic modes, transforming in $D_{3d}$ symmetry as $E_u$ and $A_{2u}$. The three infrared-active modes also transform as $E_u$ and $A_{2u}$. The Raman modes are characterized as $E_g$ and $A_{1g}$. The $E$ modes have atomic displacements parallel to $x$ and $y$, the $A$ modes displacements parallel to $z$.

For a proper analysis of the vibronic coupling the normal vibrations of the crystal as modified by the impurity ion should be used. This requires solving the full dynamical matrix of host lattice plus impurity ion. An analysis of this type has not been given so far, and explicit expressions of the normal modes are not available. In this section we will employ a highly simplified model of vibrational modes. In the first place we neglect the specific influence of the impurity ion, i.e., we assume the same vibrations as for the pure host crystal. This corresponds not only to neglecting local modes and gap modes, but also to neglecting local modifications of the normal coordinates in the vicinity of the impurity ion. Secondly, we assume that the nine phonon branches do not mix. This is a very crude approximation, which is certainly not valid at points in the Brillouin zone where branches are close to one another. Finally, we consider only vibrations within one $MI_2$ slab, i.e., we neglect dispersion of lattice vibrations in the direction parallel to the $c$ axis.

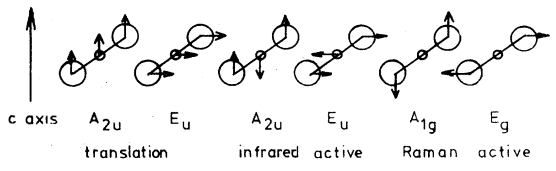


FIG. 6. Nine normal modes at $\vec{k}=0$ of the $Cd(OH)_2$ structure.

The local amplitudes of the metal $\vec{u}_M$ and of the iodine atoms $\vec{u}_L$ and $\vec{u}_{L'}$ are

$$u_M^{n\alpha} = \sum_k \sum_i C_{Mi}^{\alpha} Q_{ki} e^{-i\vec{k}\cdot\vec{n}} , \tag{17}$$

$$u_L^{n\alpha} = \sum_k \sum_i C_{Li}^{\alpha} Q_{ki} e^{-i\vec{k}\cdot\vec{n}} , \tag{18}$$

$$u_{L'}^{n\alpha} = \sum_k \sum_i C_{L'i}^{\alpha} Q_{ki} e^{-i\vec{k}\cdot\vec{n}} , \tag{19}$$

where $\vec{n} = n_1\vec{a}_1 + n_2\vec{a}_2$ denotes the two-dimensional unit cell, $\alpha$ describes the Cartesian $x$, $y$, and $z$ axes, $M$ is the mass of the metal ion and $m$ is the mass of the anion. The assumptions correspond to using $k$-independent coefficients $C$; the $\vec{k}$ dependence of the displacements is restricted to the phase factor $e^{-i\vec{k}\cdot\vec{n}}$.

The coefficients $C$ are readily calculated from the $\vec{k}=0$ modes. For the acoustic modes ($i=1-3$) we obtain

$$C^{\alpha}_{Mi}=C^{\alpha}_{Li}=C^{\alpha}_{L'i}=N^{-1/2}(M+2m)^{-1/2} \quad . \tag{20}$$

For the infrared modes ($i=4-6$) the coefficients are

$$\begin{aligned} C^{\alpha}_{Mi}&=N^{-1/2}M^{-1}[1/M+1/(2m)]^{-1/2} \quad , \\ C^{\alpha}_{Li}&=C^{\alpha}_{L'i}=-N^{-1/2}(2m)^{-1}[1/M+1/(2m)]^{-1/2} \quad . \end{aligned} \tag{21}$$

The Raman modes ($i=7-9$) have coefficients

$$\begin{aligned} C^{\alpha}_{Mi}&=0 \quad , \\ C^{\alpha}_{Li}&=-C^{\alpha}_{L'i}=N^{-1/2}(2m)^{-1/2} \quad . \end{aligned} \tag{22}$$

In these formula $N$ is the number of unit cells per unit volume.

In the previous section we emphasized that the modulation of the metal-ligand distance is mainly responsible for the coupling of the vibrations with the electronic transition. The next step is to write the three components of the local distortion $t_{1u}$ of the $NiI_6^{4-}$ octahedron in terms of atomic displacements of $Ni^{2+}$ and the six ligand iodine ions. Then, using Eqs. (17)–(22), it is possible to derive expressions for the local $t_{1u}$ distortion of the $NiI_6^{4-}$ octahedron in terms of the normal coordinates of the crystal. In this way the coefficients $S^{\rho}_{ki}$ of Eq. (6) are calculated.

The site symmetry of the $Ni^{2+}$ ion in $CdI_2$ and $PbI_2$ is not octahedral, but rather $D_{3d}$. As the trigonal field is small its influence on the electronic states can be neglected, and the electronic states can be labeled according to their $O_h$ representation. On the other hand, it is well known that the influence of the trigonal field, especially the influence of the static dipoles at the iodine ions, on the vibrational frequencies and oscillator strengths is appreciable.[17,18] Therefore, a localized $t_{1u}$ distortion should be decomposed into $a_{2u}$- and $e_u$-type distortions (site symmetry $D_{3d}$). The $\rho=0$ component of $t_{1u}$ corresponds to $a_{2u}$ and the $\rho=\pm1$ components to $e_u$. It is expected that this anisotropy will lead to different vibronic coupling strengths for $t_{1u}(0)$ and $t_{1u}(\pm1)$. Hence, we introduce a factor $g$ which expresses this anisotropy of the coupling:

$$\begin{aligned} &\langle {}^3T_{2u}M_s\kappa|\Delta U^{t_{1u}}_{\rho}|{}^3T_{1g}M_sj\rangle \propto \langle {}^3T_{2u}||\Delta U^{t_{1u}}||{}^3T_{1g}\rangle \\ &\qquad\qquad \text{for } \rho=0 \quad , \\ &\langle {}^3T_{2u}M_s\kappa|\Delta U^{t_{1u}}_{\rho}|{}^3T_{1g}M_sj\rangle \propto g\,\langle {}^3T_{2u}||\Delta U^{t_{1u}}||{}^3T_{1g}\rangle \\ &\qquad\qquad \text{for } \rho=\pm1 \quad . \end{aligned} \tag{23}$$

The result is that all transition moments which involve a $t_{1u}(\pm1)$ component (Table I) are multiplied by a factor $g^2$.

To illustrate the effect of the anisotropy we calculate first the absorption coefficients $\epsilon_{\parallel}(\vec{E}\parallel c)$ and $\epsilon_{\perp}(\vec{E}\perp c)$ for the hypothetical case of a single isolated octahedron $NiI_6^{4-}$ with the static dipoles $\vec{m}_0(\parallel c)$ at the iodine ions. The dipoles cause a splitting of the $t_{1u}$ vibration into two components $a_{2u}(\omega_{\parallel},q_0)$ and $e_u(\omega_{\perp},q_{\pm1})$, respectively. The ratio $\epsilon_{\perp}/\epsilon_{\parallel}$ for coupling with ${}^3T_{1g}$ and ${}^3T_{2g}$ can be calculated from the transition moments given in Table I, including the factor $g$:

$$\epsilon_{\perp}/\epsilon_{\parallel}=(5g^2+1)/(2g^2+4) \tag{24a}$$

for coupling with ${}^3T_{1g}$

$$\epsilon_{\perp}/\epsilon_{\parallel}=(g^2+1)/2g^2 \tag{24b}$$

for coupling with ${}^3T_{2g}$. In Appendix A we will show that the modulation of the crystal-field potential produces an anisotropic coupling with $g^2>>1$. Therefore, the fact that the $\alpha$-polarized spectrum is more intense than the $\pi$-polarized spectrum indicates that the coupling of the ${}^1E_g$ occurs mainly with the $E_g({}^3T_{1g})$ state (Fig. 7). The theoretical ratio $\epsilon_{\perp}/\epsilon_{\parallel}$ is 2.5 ($g^2>>1$), in very good agreement with the observed ratio 2.4. This is also consistent with the observed positive MCD for the vibronic side band (coupling with ${}^3T_{1g}$ gives a positive, coupling with ${}^3T_{2g}$ a negative MCD signal).

The evaluation of the MCD sign and dipole strength of the $a^4T_{1g}\rightarrow b^2T_{1g}$, ${}^2A_{1g}$ transitions in $CdI_2$:$Co^{2+}$ is less straightforward, because there are four possible ungerade intermediate states, which couple the $b^4T_{1g}$ states with a $t_{1u}$ distortion.[10]

We are now in a position to evaluate the separate contributions of the modes in the Brillouin zone (Fig. 8). We have calculated integrated intensities and the separate contributions of the modes as a function of $\vec{k}$ for the high-symmetric directions in the Brillouin

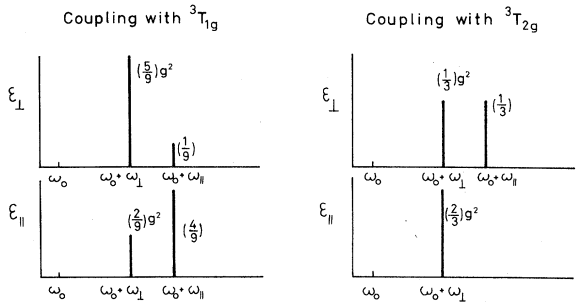


FIG. 7. Diagram showing the relative contribution of $a_{2u}(\omega_{\parallel})$ and $e_u(\omega_{\perp})$ vibrational components to the ${}^3A_{2g}\rightarrow{}^1E_g$ transition in $CdI_2$:$Ni^{2+}$ for light polarized parallel ($\epsilon_{\parallel}$) or perpendicular ($\epsilon_{\perp}$) to the trigonal axis.

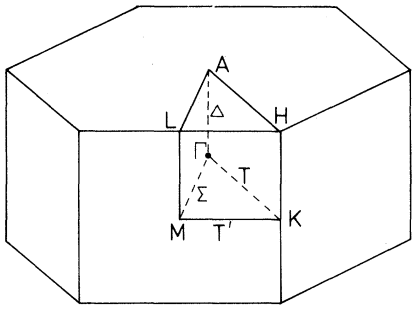


FIG. 8. Brillouin zone for the hexagonal Bravais lattice with symmetry lines and points, labeled according to the standard notation. For $M\vec{k}=(0,\frac{1}{2},0)$, for $K\vec{k}=(\frac{2}{3},\frac{1}{3},0)$.

zone. The quantity

$$A_{ki}^{\beta}=\sum_{\rho}\sum_{\rho'}(S_{ki}^{\rho})^{*}S_{ki}^{\rho'}\sum_{a\to b}(B_{ab}^{\beta\rho})^{*}B_{ab}^{\beta\rho'} \tag{25}$$

describes the contribution of one particular mode $i$ with wave vector $\vec{k}$ to the absorption coefficient. The contributions to the intensities of the polarized spectra, $\vec{E}\parallel c$ and $\vec{E}\perp c$, are $A_{ki}^{\parallel}=A_{ki}^{0}$ and $A_{ki}^{\perp}=\frac{1}{2}(A_{ki}^{1}+A_{ki}^{-1})$. For coupling with ${}^3T_{1g}$ we find from Table I (with $A=M_1^2/324$):

$$\begin{aligned}A_{ki}^{\parallel}&=2A\left[g^2\sum_{\rho}|S_{ki}^{\rho}|^2+(4-g^2)|S_{ki}^{0}|^2\right],\\ A_{ki}^{\perp}&=2A\left[\tfrac{5}{2}g^2\sum_{\rho}|S_{ki}^{\rho}|^2+(1-\tfrac{5}{2}g^2)|S_{ki}^{0}|^2\right].\end{aligned} \tag{26}$$

The total contribution of the acoustic modes ($i=1-3$) to the polarized spectra is obtained from the explicit expressions for $S_{ki}^{\rho}$

$$A_{k1}^{\parallel}+A_{k2}^{\parallel}+A_{k3}^{\parallel}=\frac{4A(4+2g^2)}{N(M+2m)}\times[(1-\cos\vec{k}\cdot\vec{a}_1)^2+(1-\cos\vec{k}\cdot\vec{a}_2)^2], \tag{27}$$

$$A_{k1}^{\perp}+A_{k2}^{\perp}+A_{k3}^{\perp}=\frac{4A(1+5g^2)}{N(M+2m)}\times[(1-\cos\vec{k}\cdot\vec{a}_1)^2+(1-\cos\vec{k}\cdot\vec{a}_2)^2]. \tag{28}$$

$\vec{a}_1$ and $\vec{a}_2$ denote primitive translations. These equations can be integrated in order to obtain the total absorption due to the acoustic modes in the $\pi$- and $\alpha$-polarized spectra:

$$A_{ac}^{\parallel}=\sum_{k}(A_{k1}^{\parallel}+A_{k2}^{\parallel}+A_{k3}^{\parallel})=\frac{12A(4+2g^2)}{(M+2m)}, \tag{29}$$

$$A_{ac}^{\perp}=\sum_{k}(A_{k1}^{\perp}+A_{k2}^{\perp}+A_{k3}^{\perp})=\frac{12A(1+5g^2)}{(M+2m)}. \tag{30}$$

The results for the infrared modes ($i=4-6$) are

$$A_{k4}^{\parallel}+A_{k5}^{\parallel}+A_{k6}^{\parallel}=\frac{4A(4+2g^2)}{N(1/M+1/2m)}\times\left[\left(\frac{1}{M}+\frac{1}{2m}\right)^2+\left(\frac{1}{M}+\frac{1}{2m}\cos\vec{k}\cdot\vec{a}_1\right)^2+\left(\frac{1}{M}+\frac{1}{2m}\cos\vec{k}\cdot\vec{a}_2\right)^2\right], \tag{31}$$

$$A_{k4}^{\perp}+A_{k5}^{\perp}+A_{k6}^{\perp}=\frac{4A(1+5g^2)}{N(1/M+1/2m)}\times\left[\left(\frac{1}{M}+\frac{1}{2m}\right)^2+\left(\frac{1}{M}+\frac{1}{2m}\cos\vec{k}\cdot\vec{a}_1\right)^2+\left(\frac{1}{M}+\frac{1}{2m}\cos\vec{k}\cdot\vec{a}_2\right)^2\right]. \tag{32}$$

The total absorption due to the infrared modes is given by

$$A_{ir}^{\parallel}=\frac{4A(4+2g^2)}{(1/M+1/2m)}\left(\frac{3}{M^2}+\frac{1}{2m^2}+\frac{1}{mM}\right), \tag{33}$$

$$A_{ir}^{\perp}=\frac{4A(1+5g^2)}{(1/M+1/2m)}\left(\frac{3}{M^2}+\frac{1}{2m^2}+\frac{1}{mM}\right). \tag{34}$$

The Raman-mode contributions are

$$A_{k7}^{\parallel}+A_{k8}^{\parallel}+A_{k9}^{\parallel}=\frac{2A(4+2g^2)}{Nm}(\sin^2\vec{k}\cdot\vec{a}_1+\sin^2\vec{k}\cdot\vec{a}_2), \tag{35}$$

$$A_{k7}^{\perp}+A_{k8}^{\perp}+A_{k9}^{\perp}=\frac{2A(1+5g^2)}{Nm}(\sin^2\vec{k}\cdot\vec{a}_1+\sin^2\vec{k}\cdot\vec{a}_2). \tag{36}$$

The total absorption due to the Raman modes is

$$A_{\text{Raman}}^{\parallel}=\frac{2(4+2g^2)A}{m}, \tag{37}$$

$$A_{\text{Raman}}^{\perp}=\frac{2(1+5g^2)A}{m}. \tag{38}$$

The integration of every branch yields the same ratio $A^{\parallel}/A^{\perp}=(4+2g^2)/(1+5g^2)$, as stated before.

In order to estimate the effect of the mass substitution of $Ni^{2+}$ in $CdI_2$, $PbI_2$, and $Co^{2+}$ in $CdI_2$ we evaluate the relative contributions of the acoustic, Raman, and infrared modes. The relative contributions are the same for the $\alpha$- and $\pi$-polarized spectrum, and depend only on the ratio $M/2m$. Figure 9 shows the result of this calculation. It is clear that the infrared modes are mainly responsible for the intensity in the spectra. However, an increase of the metal-ion mass leads to a strong reduction of the infrared-mode contribution and an enhancement of

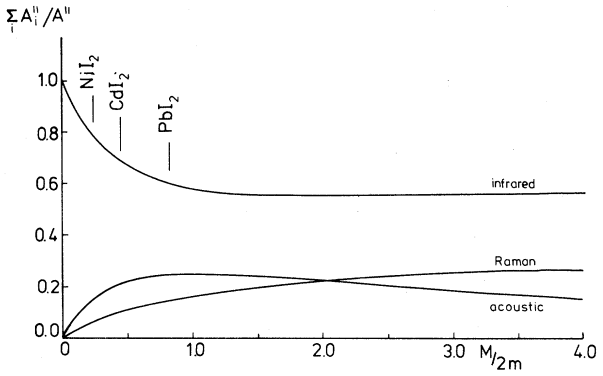


FIG. 9. Contributions of the acoustic, Raman, and infrared mode branches to the intensity of the vibronic side bands of the ${}^3A_{2g} \rightarrow {}^1E_g$ transition in $NiI_2$, $CdI_2$:$Ni^{2+}$, and $PbI_2$:$Ni^{2+}$ as a function of $M/2m$.

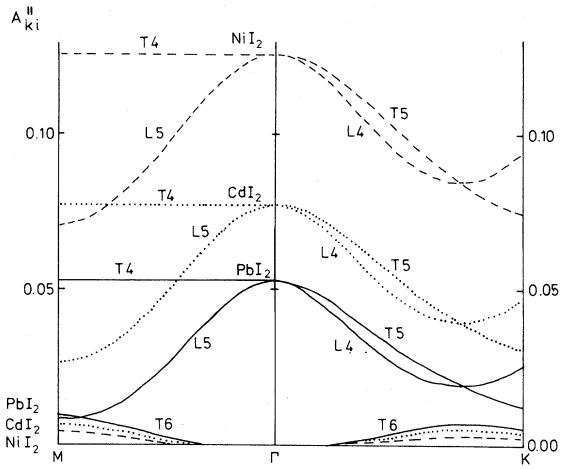


FIG. 11. Contributions (for $g^2 >> 1$) of the infrared modes $i = 4-6$, as a function of $k$, calculated for $NiI_2$(– – –), $CdI_2$(· · · ·), and $PbI_2$(——); $A_{ki}^{\perp} = \frac{5}{2} A_{ki}^{II}$ (in units $2Ag^2 N_0 N^{-1}$; $N_0$ is Avogadro's number).

that of the acoustic modes. The Raman modes appear rather weakly in the spectra.

Maxima in the absorption are expected from flat regions at symmetry points in the Brillouin zone, where we can sum over a large number of $\vec{k}$ values in a narrow frequency range. We have calculated $A_{ki}^{II}(i = 1-9)$ as a function of $\vec{k}$ for $\Gamma \rightarrow M$ and $\Gamma \rightarrow K$. In Fig. 10 the contributions of the acoustic and Raman modes are shown. Transverse or longitudinal modes are indicated by the $T$ and $L$, respectively. In Fig. 11 the infrared-mode contributions are shown; it is necessary in this case to include explicitly the masses of Ni, Cd, Pb, and I.

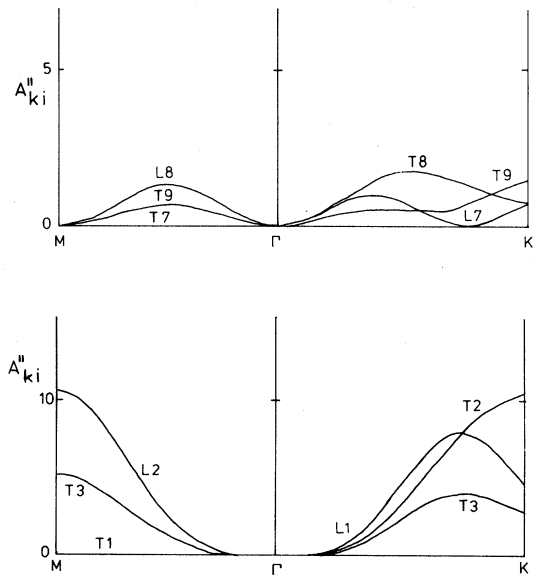


FIG. 10. Contributions (for $g^2 >> 1$) of the acoustic modes $i = 1-3$ [lower part; in units $2Ag^2 N^{-1}(M+2m)^{-1}$] and Raman modes $i = 7-9$ (upper part; in units $2Ag^2 N^{-1} m^{-1}$) as a function of $k$; $A_{ki}^{\perp} = \frac{5}{2} A_{ki}^{II}$.

From $\Gamma \rightarrow M$ the acoustic mode $T1(\parallel x)$ and the Raman mode $T7$ do not give rise to any absorption. Figure 11 illustrates the small contribution of $T6(\parallel z)$-type modes for $NiI_2$, $CdI_2$, and $PbI_2$. In the latter compound the absorption is much weaker than in the others. The difference between absorption due to the displacements in the $x$, $y$, and $z$ direction, respectively, is the smallest in $PbI_2$.

## IV. DISCUSSION

In previous sections we have shown that the maxima of absorption due to one-phonon electric-dipole transitions are expected to correspond to maxima in the phonon density of states of the host crystal. In this section we will assign the observed maxima to phonons corresponding to specific points in the Brillouin zone.

The phonon frequencies of $CdI_2$, $PbI_2$, $CoI_2$, and $NiI_2$ are given in Table II.[18–22] The Raman frequencies of $CoI_2$ and $NiI_2$ are not known; the frequencies given in Table II are those reported for $VI_2$; these are probably not very different from the frequencies of $CoI_2$ and $NiI_2$. The phonon frequencies of $NiI_2$ and $CoI_2$ are presumably reduced in $CdI_2$:$Ni^{2+}$ and $CdI_2$:$Co^{2+}$, due to smaller force constants and larger induced static dipoles at the iodine ions.[17] Therefore we do not expect that the incorporation of $Ni^{2+}$ and $Co^{2+}$ in $CdI_2$ leads to local modes. The optical frequencies of $NiI_2$ and $PbI_2$ are quite different, but because the effective ionic radius of $Pb^{2+}$ (1.18 Å) is

TABLE II. Experimental optical frequencies ($\vec{k}=0$) in units of $cm^{-1}$ of $CoI_2$, $NiI_2$, $CdI_2$, and $PbI_2$. The references from which the data were taken, are given.

| Optical modes | $CoI_2$ | Ref. | $NiI_2$ | Ref. | $CdI_2$ | Ref. | $PbI_2$ | Ref. |
|---|---|---|---|---|---|---|---|---|
| $E_u^{TO}$ | 152 | | 156 | | 79 | | 52 | |
| | | 22 | | 18 | | 20 | | 20 |
| $E_u^{LO}$ | 175 | | 176 | | 132 | | 108 | |
| $A_{2u}^{TO}$ | 185 | | 178 | | 136 | | 96 | |
| | | 22 | | 18 | | 20 | | 20 |
| $A_{2u}^{LO}$ | 191 | | 184 | | 152 | | 121 | |
| $E_g$ | ~90 | | ~90 | | 44 | | 74 | |
| | | 19 | | 19 | | 21 | | 21 |
| $A_{1g}$ | ~115 | | ~115 | | 112 | | 96 | |

much larger than that of $Ni^{2+}$ (0.700 Å),[23] force constants will be strongly reduced in $PbI_2$:$Ni^{2+}$.

For the assignment of the maxima in the vibronic spectra the compatibility relations are indispensable. These relations show how the space-group representations of the branches in the various directions of the Brillouin zone are connected. The compatibility relations for the $Cd(OH)_2$ structure, space group $D_{3d}^3$, calculated with help of the character tables,[24] are listed in Table III for a number of symmetry lines and points.

Because phonon dispersion curves of $PbI_2$ have been calculated[21,25] and partly measured,[26,27] we begin to assign the maxima of the spectra of the $^3A_{2g} \rightarrow {}^1E_g$ in $PbI_2$:$Ni^{2+}$ (Fig. 2). The weak band at 12 394 $cm^{-1}$, which has a MCD sign opposite to that of the vibronic side band, is assigned to the zero-phonon transition. According to the overall positive MCD signal the main contributions arise from a $e_u$-type distortion (Table I); the coupling with $a_{2u}$ would give a negative MCD. The positions of the maxima of the vibronic side bands, relative to the frequency of the zero-phonon band, are listed in Table IV. The maxima are assigned to space-group representations corresponding mostly to $M$ and $K$ points in the Brillouin zone. The listed experimental (neutron scattering) and calculated frequencies are obtained from Dorner,[26] Prévot,[27] and Frey,[21] respectively. Estimat-

TABLE III. Compatibility relations of the $Cd(OH)_2$ structure. The points and lines in the Brillouin zone are given in standard notation, together with the appropriate factor group and the degeneracy of the star of $\vec{k}$. For clearness' sake the point-group representations are given. The mode numbers are those given in Sec. III C.

| Point or line | Γ | Σ | $M$ | $T'$ | $K$ | $T$ | Γ | Δ | $A$ |
|---|---|---|---|---|---|---|---|---|---|
| Point group | $D_{3d}$ | $C_{1h}$ | $C_{2h}$ | $C_2$ | $D_3$ | $C_2$ | $D_{3d}$ | $C_{3v}$ | $D_{3d}$ |
| Degeneracy | 1 | 6 | 3 | 6 | 2 | 6 | 1 | 2 | 1 |
| Mode 1,4 | $E_u$ | $A''$ | $A_u$ | $A$ | $E$ | $A''$ | $E_u$ | $E$ | $E_u$ |
| 2,5 | | $A'$ | $B_u$ | $B$ | | $A'$ | | | |
| 3,6 | $A_{2u}$ | $A'$ | $B_u$ | $B$ | $A_2$ | $A'$ | $A_{2u}$ | $A_1$ | $A_{2u}$ |
| Mode 7 | $E_g$ | $A'$ | $A_g$ | $A$ | $E$ | $A'$ | $E_g$ | $E$ | $E_g$ |
| 8 | | $A''$ | $B_g$ | $B$ | | $A''$ | | | |
| 9 | $A_{1g}$ | $A'$ | $A_g$ | $A$ | $A_1$ | $A'$ | $A_{1g}$ | $A_1$ | $A_{1g}$ |

TABLE IV. Assignments of the maxima of the $^3A_{2g} \rightarrow {}^1E_g$ transition of $PbI_2:Ni^{2+}$ to vibrational modes listed according to their space-group representation. The corresponding point-group representations of $D_{3d}$ are also given. A comparison between the relative positions in the vibronic spectrum with respect to the zero-phonon band ($\nu_0 = 12\,394$ cm$^{-1}$) and experimental (Refs. 26 and 27) and calculated (Ref. 21) phonon frequencies of $PbI_2$ is made.

| Relative position (cm$^{-1}$) | Space-group representation | Expt. (*) or calc. frequency (cm$^{-1}$) | Point-group $D_{3d}$ representation |
|---|---|---|---|
| 22 | $L_4$ | | $E_u + A_{2u}$ |
| | $K_2$ | 22* | $A_{2u} + A_{2g}$ |
| 28 | $M_4$ | 29* | $E_u + A_{2u}$ |
| 44 | $K_3$ | 45* | $E_u + E_g$ |
| 49 | $M_4$ | 50* | $E_u + A_{2u}$ |
| 54 | $K_2$ | 54 | $A_{2u} + A_{2g}$ |
| | $M_2$ | 56* | $E_u + A_{1u}$ |
| 69 | $K_3$ | 66 | $E_u + E_g$ |
| | $A_3$ | 68 | $E_g$ |
| | $M_1$ | 71* | $E_g + A_{1g}$ |
| | $M_3$ | 71* | $E_g + A_{2g}$ |
| 80 | $K_1$ | 78 | $A_{1g} + A_{1u}$ |
| | $M_1$ | 83 | $A_{1g} + E_g$ |
| 91 | $A_1$ | 91 | $A_{1g}$ |
| 110 | $E_u^{LO}\Sigma_1$ | 104 | $E_u$ |
| | $E_u^{LO}T_1$ | | $E_u$ |
| 117 | $A_{2u}^{LO}\Delta_1$ | 118 | $A_{2u}$ |
| | $M_4$ | 119 | $E_u + A_{2u}$ |

ed errors amount to a few wave numbers. The agreement between the positions in the spectrum $PbI_2:Ni^{2+}$ and the experimental and calculated frequencies of the modes in $PbI_2$ is good.

Due to the low frequency of the $E_u^{TO}$ mode (52 cm$^{-1}$) and the strongly reduced nearest-neighbor force constants, the low-energy part of the spectrum is enhanced in intensity. As the main contributions arise from the $E_u$ modes (positive MCD signal), the peak at 22 cm$^{-1}$ should be assigned to $L_4$, because $K_2(A_{2u}^{TA})$ would produce a negative MCD. The mode frequency at $L_4$ is not known, but can be estimated from the acoustic mode at $M$ and $A$,[21] which have frequencies of 29 and 14 cm$^{-1}$, respectively.

The bands at about 69 and 80 cm$^{-1}$ are weak; although the contribution of the Raman modes at point $M$ was calculated to be zero, some intensity may be obtained on the $\Sigma$ line, where mixing of ungerade and gerade modes is allowed. Surprisingly large is the peak intensity at 91 cm$^{-1}$. We do not understand the large intensity of this mode; the frequency corresponds to an $A_{1g}$ mode at the $\Gamma$ point.

The vibronic bands of the $^3A_{2g} \rightarrow {}^1E_g$ transition in $CdI_2:Ni^{2+}$ are shown in Fig. 1 and Table V. The weak band at 12 441 cm$^{-1}$ was assigned to the zero-phonon transition. The vibronic frequencies obtained from the $CdI_2:Ni^{2+}$ spectrum are compared in Table V with the frequencies obtained from the $CdI_2:Co^{2+}$ $a^4T_{1g}(E_g') \rightarrow b^2T_{1g}(U_g', E_g')$ transitions (Fig. 3). The absorptions at 15 280 and 15 376 cm$^{-1}$ were assigned

TABLE V. Assignment of the maxima in the vibronic spectra of $CdI_2$:$Co^{2+}$ for the transitions $a^4T_{1g}(E_g') \rightarrow b^2T_{1g}(U_g')$($\nu_0$ = 15 280 $cm^{-1}$), $a^4T_{1g}(E_g') \rightarrow b^2T_{1g}(E_g')$ ($\nu_0$ = 15 376 $cm^{-1}$), and of $CdI_2$:$Ni^{2+}$ for the transition $^3A_{2g}(T_{2g}) \rightarrow {}^1E_g(E_g)$($\nu_0$ = 12 441 $cm^{-1}$). Positions of the vibronic maxima are given (in $cm^{-1}$) relative to the zero-phonon origin $\nu_0$.

| $CdI_2$:$Co^{2+}$ $\nu_0$ = 15 280 | $CdI_2$:$Co^{2+}$ $\nu_0$ = 15 376 | $CdI_2$:$Ni^{2+}$ $\nu_0$ = 12 441 | Space-group representation | Point-group $D_{3d}$ representation |
|---|---|---|---|---|
| . . . | . . . | . . . | $L_4$ | $E_u + A_{2u}$ |
| | | | $K_2$ | $A_{2u} + A_{2g}$ |
| 35 | . . . | 37 | $K_3$ | $E_u + E_g$ |
| | | | $M_3$ | $E_g + A_{2g}$ |
| 60 | 64 | 59 | $M_4$ | $E_u + A_{2u}$ |
| | | | $(M_1)$ | $E_g + A_{1g}$ |
| 68 | 72 | 67 | $K_3$ | $E_u + E_g$ |
| 78 | 79 | | $M_2$ | $E_u + A_{1u}$ |
| | | 76 | $E_u^{TO}\Delta_3$ | $E_u$ |
| 87 | 89 | | $K_3$ | $E_u + E_g$ |
| | | | $M_2$ | $E_u + A_{1u}$ |
| 107 | 108 | 99 | $K_1$ | $A_{1u} + A_{1g}$ |
| | | | $(M_1)$ | $A_{1g} + E_g$ |
| 112 | 112 | 103 | $M_4$ | $A_{2u} + E_u$ |
| | | | $K_2$ | $A_{2u} + A_{2g}$ |
| 129 | 129 | 117 | $K_3$ | $E_u + E_g$ |
| | | | $M_4$ | $E_u + A_{2u}$ |
| 138 | 138 | 131 | $E_u^{LO}\Sigma_1$ | $E_u$ |
| | | | $E_u^{LO}T_1$ | $E_u$ |

to the zero-phonon transitions. The two transitions are intraconfigurational transitions within the strong-field configuration $t_{2g}^5e_g^2$.

The phonon dispersion curves of $CdI_2$ are not known. Calculations are not available, and the experimental determination with inelastic neutron scattering is hampered by the large neutron absorption of Cd. We have used the observed maxima of the vibronic spectra to estimate the phonon dispersion curves of $CdI_2$. For this purpose we have used the frequencies of the zone-center modes (Table II), the compatibility relations (Table III), and also the comparison with $PbI_2$. An important difference between the phonon branches of $CdI_2$ and $PbI_2$ is caused by the reversal of the $E_u^{TO}$ and $E_g$ frequencies.

From these considerations the vibrational branches of $CdI_2$ have been deduced, as shown in Fig. 12. The assignment of the observed maxima is given in Table V. Weak absorptions due to acoustic and Raman modes are observed only in a few cases. Those modes at the $M$ point which have been calculated zero are put between brackets (fifth column of Table V). A possible peak at 99 $cm^{-1}$ in the spectrum of the $a^4T_{1g}(E_g') \rightarrow b^2T_{1g}(U_g')$ transition is overlapped by the zero-phonon band of the $b^2T_{1g}(E_g')$ transition.

The correspondence between the spectra is remarkable, and it shows indeed that the host lattice $CdI_2$ is responsible for the observed fine structure. The spectrum of the $a^4T_{1g} \rightarrow {}^2A_{1g}$ is broadened and presumably also shows contributions of two-phonon processes (Fig. 4).

As shown by the calculation in the previous section

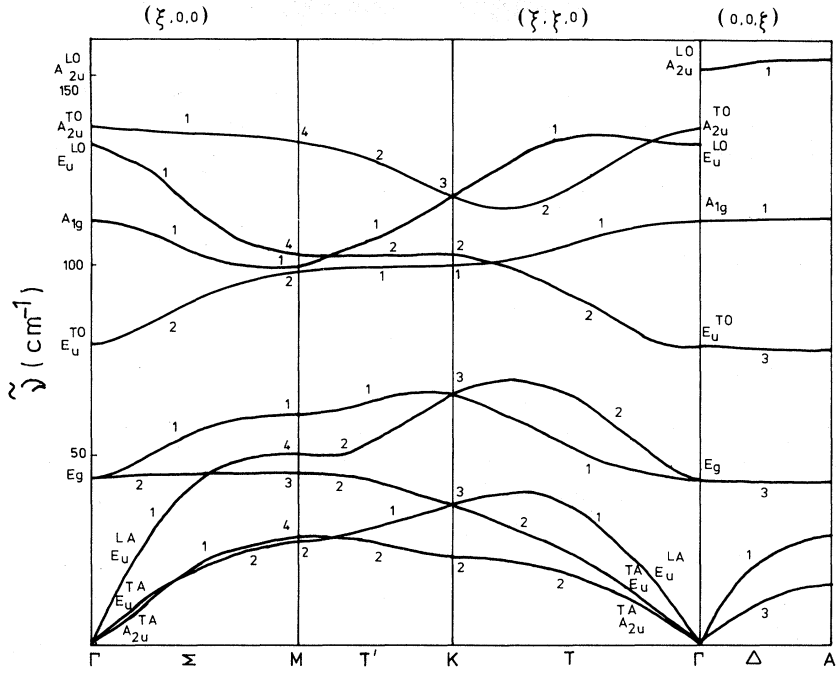


FIG. 12. Dispersion of the acoustic and optic branches of $CdI_2$ as deduced from the vibronic fine structure of the ${}^3A_{2g} \rightarrow {}^1E_g$ transition. The numbers indicate the space-group representation.

a reduction of the intensities from $\alpha$ to $\pi$ polarization of about 60% is expected for the ${}^3A_{2g} \rightarrow {}^1E_g$ transition, if the coupling of ${}^1E_g$ is mainly with the ${}^3T_{1g}$ state (Fig. 1) and the vibronic coupling is due to the $e_u$ component of the $t_{1u}$ distortions. A positive MCD is calculated in this case as is observed for the entire vibronic spectrum of the ${}^3A_{2g} \rightarrow {}^1E_g$ transition. An exception is the band at 12 544 $cm^{-1}$ which does not reduce in intensity from $\alpha$ to $\pi$ polarization. This band is assigned to a mainly $A_{2u}$-type vibration. For a pure $A_{2u}$-type contribution, an enhancement of the intensity by a factor 4 from $\alpha$ to $\pi$ polarization is expected. We remark that the selection rules are not strictly valid; at arbitrary points in the Brillouin zone, mixing of all vibrational modes occurs, and this will lead to (small) contributions of other modes to the vibronic side band.

The ${}^4T_{1g} \rightarrow {}^2A_{1g}$ transition shows a very narrow $\sigma$-polarized band at 47 $cm^{-1}$ with respect to $\nu_0 = 15\,669$ $cm^{-1}$. The origin of this peak is not clear; it could be related to a local mode.

## ACKNOWLEDGMENTS

This investigation was supported by the Netherlands Foundation for Chemical Research (SON) with financial aid from the Netherlands Organization for the Advancement of Pure Research.

## APPENDIX A: MODULATION OF THE CUBIC CRYSTAL-FIELD POTENTIAL BY A $t_{1u}$ VIBRATION

In order to calculate the matrix elements of the vibronic coupling operator $\langle {}^{2S+1}\Gamma_u | U | {}^{2S+1}\Gamma_g' \rangle$, the change of the crystal field due to $t_{1u}$ vibrations has to be evaluated. For this we use the polarizable-ion model in which the metal ion has an effective (Szigeti) charge $+2Z$ and the anions a charge $-Z$; the electronic polarizability of the anions is $\alpha$.

The matrix elements contain wave functions which are defined with respect to the position $\vec{R}_M$ of the central metal atom:

$$\langle {}^{2S+1}\Gamma_u(\vec{r}-\vec{R}_M) | U(\vec{r}) | {}^{2S+1}\Gamma_g'(\vec{r}-\vec{R}_M) \rangle \ . \quad \text{(A1)}$$

We define a coordinate $\vec{r}'$ which gives the position of the electron with respect to the cation nucleus: $\vec{r}' = \vec{r} - \vec{R}_M$. We consider contributions to $U(\vec{r})$ from the charges $Z_i$ and the induced dipoles $\vec{m}_i$ on ligand ions $i$. Only nearest neighbors are considered ($i = 1-6$).

$$U(r) = \sum_i \frac{Z_i e}{|\vec{r}-\vec{R}_i|} + \sum_i \frac{\vec{m}_i \cdot (\vec{r}-\vec{R}_i)}{|\vec{r}-\vec{R}_i|^3} \ . \quad \text{(A2)}$$

We evaluate the change $\Delta U$ caused by small displacements $u_{i\alpha}$ and $u_{M\alpha}$ of the nuclei from the equilibrium positions $\vec{R}_i^0$ and $\vec{R}_M^0$:

$$R_{i\alpha} = R_{i\alpha}^0 + u_{i\alpha} \ , \quad R_{M\alpha} = R_{M\alpha}^0 + u_{M\alpha} \ , \quad \text{(A3)}$$

with $\alpha = x,y,z$. We choose the equilibrium position of the central metal ion as the origin, which means that $\vec{R}_M^0 = 0$ and $R_{M\alpha} = u_{M\alpha}$. Equation (A2) is now expanded and the terms linear in the displacements are retained. There is a term in $\Delta U$ which arises from the change of the induced dipole moments by the vibration. The total induced moment is $\vec{m}_i = \alpha \vec{E}_i$ where $\vec{E}_i$ is the total electric field at ligand $i$, position $\vec{R}_i$. The field $\vec{E}_i$ is also expanded in small displacements of the nuclei, which results in an extra contribution to $\Delta U$. From this term and the expansion of Eq. (A2) we obtain for a $t_{1u}$ vibration

$$\Delta U^{t_{1u}}(\vec{r}' + \vec{R}_M) = \sum_i \sum_\alpha G_{i\alpha}(u_{i\alpha} - u_{M\alpha}) \ , \qquad \text{(A4)}$$

where we have substituted $Z_i = -Z$ and $Z_M = +2Z$ and $|\vec{R}_i^0| = \vec{R}_0$. Ignoring terms with $(u_{i\alpha} - u_{j\alpha})$ which do not contribute to a $t_{1u}$ vibration, $G_{i\alpha}$ is given by

$$G_{i\alpha} = -\frac{Ze(r'_\alpha - R^0_{i\alpha})}{|\vec{r}' - \vec{R}_i^0|^3} - \frac{m_{i\alpha}}{|\vec{r}' - \vec{R}_i^0|^3} + \sum_\beta \frac{3m_{i\beta}(r'_\beta - R^0_{i\beta})(r'_\alpha - R^0_{i\alpha})}{|\vec{r}' - \vec{R}_i^0|^5} - \frac{2Ze\alpha(r'_\alpha - R^0_{i\alpha})}{R_0^3 |\vec{r}' - \vec{R}_i^0|^3} + 6Ze\alpha \sum_\beta \frac{R^0_{i\alpha} R^0_{i\beta}(r'_\beta - R^0_{i\beta})}{R_0^5 |\vec{r}' - \vec{R}_i^0|^3} \ . \qquad \text{(A5)}$$

The function $G_{i\alpha}(\vec{r}')$ is now expanded for small values of $\vec{r}'$ and only terms linear in $\vec{r}'$ are retained. The $G_{i\alpha}$ terms may then be calculated by substituting values of the coordinates $R^0_{i\alpha}$ and the dipole moments $m_{i\alpha}$. The displacements $u_{i\alpha}$ and $u_{M\alpha}$ are transformed to the $t_{1u}$ normal coordinates $q_0$ and $q_{\pm 1}$. The resulting expression for the modulation of the crystal field due to a $t_{1u}$ vibration is

$$\Delta U^{t_{1u}} = Cr'_z q_0 + gC(\omega r'_- q_1 + \omega^2 r'_+ q_{-1}) \ , \qquad \text{(A6)}$$

with

$$C = \frac{2Ze\sqrt{6}}{3R_0^3}\left(1 - \frac{4\alpha}{R_0^3}\right); \quad \omega = \exp(\tfrac{2}{3}\pi i) \ ,$$

and

$$g = 1 + \frac{3m_0\sqrt{3}}{2ZeR_0}\left(\frac{1}{1 - (4\alpha/R_0^3)}\right) \ .$$

An anisotropic coupling results, if $g$ deviates from one. This anisotropy is due to the static dipole moments $m_0$ at the iodine ions and is independent of the magnitude of the charge $Z$ ($m_0$ is proportional to $Z$).

With use of the values of $NiI_2$,[18] $CdI_2$,[17] and $PbI_2$,[17] for the parameter $\alpha$, $g$ is calculated as $-8.35$ for $NiI_2$, $+6.49$ for $CdI_2$, and $+7.59$ for $PbI_2$. This shows that the coupling is very anisotropic in these cases, with stronger coupling to the $e_u(t_{1u} \pm 1)$ modes than to the $a_{2u}(t_{1u}0)$ modes.


[1] R. W. G. Wyckhoff, *Crystal Structures* (Interscience, New York, 1963), Vol. 1.

[2] W. E. Bron and M. Wagner, Phys. Rev. A 139, 233 (1965).

[3] R. A. Satten, J. Chem. Phys. 40, 1200 (1964).

[4] A. S. Barker and A. J. Sievers, Rev. Mod. Phys. 47, Suppl. No. 2, S1 (1975).

[5] N. B. Manson and K. Y. Wong, J. Phys. C 8, L73 (1975).

[6] N. B. Manson and K. Y. Wong, J. Phys. C 9, 611 (1976).

[7] M. J. L. Sangster and C. W. McCombie, J. Phys. C 3, 1498 (1970).

[8] S. R. Kuindersma and P. R. Boudewijn, Solid State Commun. 27, 1181 (1978).

[9] P. R. Boudewijn, thesis (Groningen, 1980) (unpublished).

[10] P. R. Boudewijn, A. Meetsma, and C. Haas, Physica (Utrecht) B 106, 165 (1981).

[11] P. N. Schatz and A. J. McCaffery, Q. Rev., Chem. Soc. 23, 552 (1969).

[12] M. Born and J. R. Oppenheimer, Ann. Phys. 84, 457 (1927).

[13] M. J. Harding, S. F. Mason, D. J. Robbins, and A. J. Thomson, J. Chem. Soc. (A) 3047 (1971).

[14] D. B. Bird, G. A. Osborne, and P. J. Stephens, Phys. Rev. B 5, 1800 (1972).

[15] J. S. Griffith, *The Irreducible Tensor Method for Molecular Symmetry Groups* (Prentice-Hall, Englewood Cliffs, 1962). The tables for the complex trigonal system contain some errors. The corrected values are

$$V\begin{pmatrix} T_1 & T_1 & T_1 \\ \alpha & \beta & \gamma \end{pmatrix} = V\begin{pmatrix} T_1 & T_2 & T_2 \\ \alpha & \beta & \gamma \end{pmatrix} = \frac{1}{\sqrt{6}}\epsilon_{\alpha\beta\gamma} \ ;$$

$$V\begin{pmatrix} E & T_1 & T_2 \\ -1 & -1 & -1 \end{pmatrix} = V\begin{pmatrix} E & T_1 & T_2 \\ 1 & 1 & 1 \end{pmatrix} = -\frac{1}{\sqrt{6}} \ .$$

[16] S. R. Kuindersma, P. R. Boudewijn, and C. Haas, Phys. Status Solidi (b) 108, 187 (1981); S. R. Kuindersma, thesis (Groningen, 1980) (unpublished).

[17] H. J. L. van der Valk and C. Haas, Phys. Status Solidi (b) 80, 321 (1977).

[18] S. R. Kuindersma, W. R. Müller, and M. Rautenberg, in the *International Conference on Lattice Dynamics,* edited by M. Balkanski (Flammarion, Paris, 1977), p. 613.

[19] G. Güntherodt, W. Bauhofer, and G. Benedek, Phys. Rev. Lett. 43, 1427 (1979).

[20] G. Lucovsky and R. M. White, Nuovo Cimento B 38, 290 (1977).

[21] A. Frey and R. Zeyher, Solid State Commun. 28, 435 (1979).

[22] S. R. Kuindersma, Phys. Status Solidi (b) 107, K163 (1981); S. R. Kuindersma, thesis (Groningen, 1980) (unpublished).

[23] R. D. Shannon and C. T. Prewitt, Acta Crystallogr., Sect. B 25, 925 (1969).

[24] C. Bradley and A. P. Cracknell, *The Mathematical Theory of Symmetry in Solids* (Clarendon, Oxford, 1972).

[25] A. Frey, thesis (Stuttgart, 1977) (unpublished).

[26] B. Dorner, R. E. Ghosh, and G. Harbeke, Phys. Status Solidi (b) 73, 655 (1976).

[27] B. Prévot, J. Biellmann, B. Dorner, and A. Frey, Solid State Commun. 35, 31 (1980).